ELSEVIER

Int. J. Therm. Sci. 41 (2002) 319–331

International Journal of Thermal Sciences

www.elsevier.com/locate/ijts

Developing laminar mixed convection with heat and mass transfer in horizontal and vertical tubes

Jamel Orfi [a], Nicolas Galanis [b,*]

[a] *Département de physique, Faculté des Sciences de Monastir, Route de Kairouan 5019, Monastir, Tunisie*
[b] *Département de génie mécanique, Université de Sherbrooke, Sherbrooke, QC, J1K 2R1, Canada*

Received 1 February 2001; accepted 9 July 2001

Abstract

The effects of the solutal and thermal Grashof numbers on the flow, temperature and concentration fields in tubes with uniform heat flux and concentration at the fluid-solid interface have been investigated numerically using a three-dimensional axially parabolic model. Results show a complex development of the flow field which is strongly influenced by the values of the two Grashof numbers and by the tube inclination. For vertical tubes the flow field is also influenced by the relative direction of the flow and the buoyancy forces. In general, very close to the tube inlet forced convection boundary layer development dominates. Further downstream, the effects of solutal buoyancy predominate while those of thermal origin determine the flow field far downstream and, in particular, the fully developed conditions. The axial evolution of the wall shear stress τ_z, the Nusselt number Nu_z and the Sherwood number Sh_z in both horizontal and vertical tubes are presented for different combinations of the two Grashof numbers. For horizontal tubes and vertical tubes with upward flow these three variables are greater than the corresponding ones for forced convection. The opposite is true for downward flow in vertical tubes.

Keywords: Mixed convection; Heat and mass transfer; Developing laminar flow; Vertical and horizontal tubes

1. Introduction

There are many natural processes and practical situations in which fluid flow occurs in the presence of temperature and/or concentration gradients: chemical distillation, evaporation from a body of water with or without wind, storage of solar energy in a saline pond, chemical vapour deposition processes, flow in heat exchangers and cooling of an airstream by evaporation are but a few examples of such situations. They indicate that the flow conditions and the geometrical configurations are extremely varied: the flow may be confined or unconfined, laminar or turbulent. It may be caused by the temperature and/or concentration gradients (natural convection) or by a mechanical appliance (forced convection). In the present study, we are specifically interested in laminar mixed convection in circular ducts.

Thermal buoyancy effects on duct flow have been studied extensively, both experimentally [1–4] and numerically [5–7] for uniform wall temperature as well as for uniform and non-uniform heat flux conditions. These and other studies (see [8]) have shown that, due to the effect of thermal buoyancy, the axial velocity profile and the isotherms are very different from those corresponding to pure forced convection.

On the other hand, mixed convection due to the combined effects of temperature and concentration gradients has received less attention. The earlier studies on the effects of mass diffusion were concerned with natural convection along a vertical flat plate [9] or a vertical cylinder [10]. Lin et al. [11] studied the effects of vaporisation of a thin liquid film wetting the inside wall of a long open-ended vertical pipe on the ascending flow therein using a two-dimensional boundary layer model. The study of Lee et al. [12] deals with the numerical prediction of mixed convection heat and mass transfer in a vertical rectangular duct with film evaporation along the porous wall. The set of equations was solved by a vorticity-velocity method for a three-dimensional parabolic flow. Yan [13] studied numerically the transport phenomena of developing laminar mixed convection with combined heat and mass transfer in inclined rectangular ducts. Typical

* Correspondence and reprints.
E-mail addresses: jamel.orfi@fsm.rnu.tn (J. Orfi), nicolas.galanis@gme.usherb.ca (N. Galanis).

1290-0729/02/$ – see front matter
PII: S1290-0729(02)01322-4

Nomenclature

a	thermal diffusivity ..... $m^2 \cdot s^{-1}$
C	dimensionless species concentration
C'	dimensional species concentration
Cp	specific heat of the fluid ..... $J \cdot kg^{-1} \cdot K^{-1}$
D	mass diffusivity ..... $m^2 \cdot s^{-1}$
D_1, D_2, D_3	different axial grid distributions
g	gravitational acceleration ..... $m \cdot s^{-2}$
Gr_c	solutal Grashof number $= \frac{g\beta^*(C'_w - C'_0)(2R)^3}{\nu^2}$
Gr_t	thermal Grashof number $= \frac{g\beta q(2R)^4}{k\nu^2}$
I_z	Ith axial step
k	thermal conductivity ..... $W \cdot m^{-1} K^{-1}$
Le	Lewis number $= D/a$
Nu_z	average Nusselt number
p	fluid pressure ..... Pa
p_m	mean cross-sectional pressure ..... Pa
p'	perturbation term about the mean pressure p_m ..... Pa
p_1	modified in plane pressure variation $= p' + \rho_0 r' g \cos\alpha \cos\theta$
p_2	modified mean cross-sectional pressure $= p_m + \rho_0 z' g \sin\alpha$
Pr	Prandtl number $= \nu/a$
q	heat flux imposed at the solid-fluid interface ..... $W \cdot m^{-2}$
r	dimensionless radial coordinate
R	tube radius
Re	Reynolds number $= \frac{V'_0 \cdot 2R}{\nu}$
Sc	Schmidt number $= \nu/D$
Sh_z	average Sherwood number
T'	fluid temperature ..... K
T	dimensionless temperature
v	dimensionless velocity
V'	fluid velocity ..... $m \cdot s^{-1}$
z	dimensionless axial coordinate

Greek symbols

α	tube inclination
β	coefficient of thermal expansion ..... K^{-1}
β^*	coefficient of concentration expansion
θ	circumferential coordinate
ν	kinematic viscosity ..... $m^2 \cdot s^{-1}$
ρ	density ..... $kg \cdot m^{-3}$
τ_z	dimensionless average shear stress

Subscripts

b	bulk fluid quantity
c	value at the centre of the tube
0	inlet conditions
r, θ, z	radial, circumferential and axial directions, respectively
w	value at the wall

Superscripts

$'$	dimensional quantity
—	average value

developments of velocity, temperature and concentration profiles were shown. The local friction coefficient as well as the Nusselt and Sherwood numbers were presented for species diffusion of interest in air ($Pr = 0.7$) over a Schmidt number range of 0.2–2. Lin et al. [14] performed a numerical study to examine the buoyancy effects of thermal and mass diffusion on laminar forced convection in the entrance region of horizontal square channels. Their results, including the developments of temperature and concentration contours, describe the effects of the bottom wall temperature and of the relative humidity on momentum, heat and mass transfer.

It is of interest to mention the recent work of Lee and Yan [15] who investigated mixed convection heat and mass transfer in radially rotating rectangular ducts. The emphasis is placed on the effects of rotation, due to the Coriolis and centrifugal forces, and mass diffusion on the flow structure and heat transfer characteristics.

This literature review shows that the problem of developing mixed convection with heat and mass transfer in the entrance region of circular ducts has not received much attention. Preliminary results corresponding to horizontal tubes were recently presented by Orfi et al. [16]. The purpose of the present study is to report detailed results on the combined effects of mass and thermal buoyancy forces on the developing laminar flow in horizontal and vertical tubes.

2. Problem formulation

We consider steady, developing, laminar flow within a long inclined circular tube of radius R subjected to a uniform heat flux q at the solid-fluid interface (Fig. 1). The fluid is a mixture of two non-reacting components (small quantity of B with large quantity of A). At the inlet section its axial velocity V'_0, temperature T'_0 and concentration C'_0 (mass of B per total mass) are uniform. All its thermo-physical properties are assumed to be constant except for the density in the body forces, which according to the Boussinesq approximation is expressed as:

$$\rho = \rho_0\left[1 - \beta\left(T' - T'_0\right) - \beta^*\left(C' - C'_0\right)\right] \quad (1)$$

The concentration C'_w at the fluid-solid interface is assumed to be uniform and not very different from C'_0.

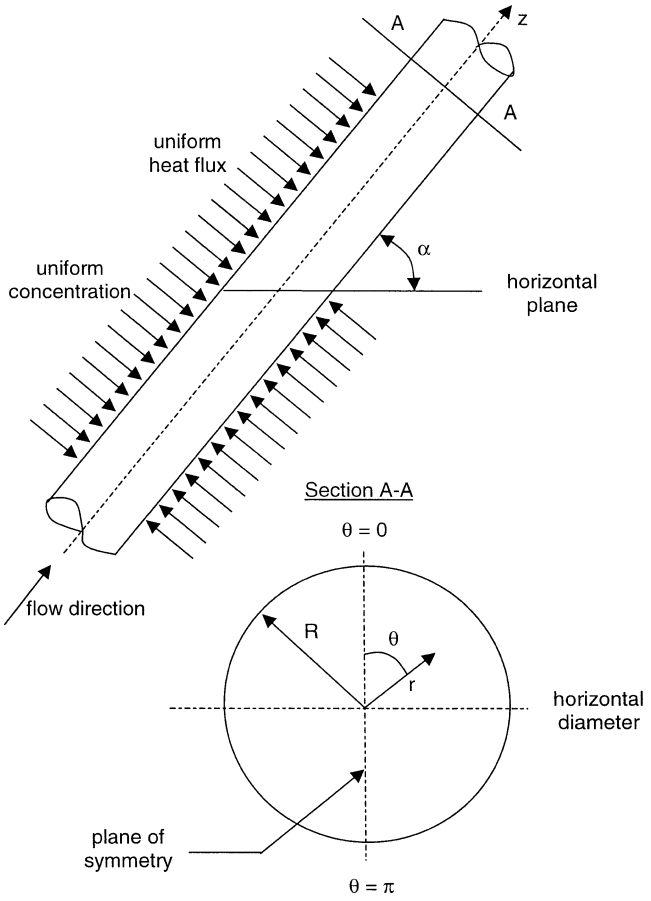

Fig. 1. Physical configuration and coordinate system.

The modelling is based on species diffusion processes with very low concentration levels such that the diffusion-thermo (Dufour) and thermo-diffusion (Soret) effects as well as the interfacial velocity due to species diffusion are neglected [9,10,17]. Viscous dissipation and axial diffusion are also considered to be negligible. The latter assumption is valid when the Peclet number is greater than 100 [13]. Finally, the upstream propagation of downstream pressure effects is neglected and the pressure can be written as:

$$p(r,\theta,z) = p_{\mathrm{m}}(z) + p'(r,\theta) \tag{2}$$

where $p_{\mathrm{m}}(z)$ is the average pressure at each axial location and $p'(r,\theta)$ is the in-plane perturbation.

It is important to mention that this pressure uncoupling and the elimination of axial diffusion in the governing equations follow the parabolic flow practice used extensively in the study of internal mixed convection problems [5,13,15, 18].

We then combine these two pressure terms with the corresponding projections of the gravity force and introduce the following nondimensional variables:

$$\begin{aligned}
&r = \frac{r'}{2R}, \qquad z = \frac{z'}{2R\,Re\,Pr}\\
&v_\theta = \frac{V'_\theta}{a/2R}, \qquad v_r = \frac{V'_r}{a/2R}, \qquad v_z = \frac{V'_z}{V'_0}\\
&P_1 = \frac{p_1}{\rho_0(a/2R)^2}, \qquad P_2 = \frac{p_2}{\rho_0 V_0'^2}\\
&T = \frac{T'-T'_0}{2Rq/k}, \qquad C = \frac{C'-C'_0}{C'_{\mathrm{w}}-C'_0}
\end{aligned} \tag{3}$$

The mass, momentum, energy and concentration equations expressed in cylindrical coordinates can then be written in the following nondimensional form:

$$\frac{1}{r}\frac{\partial(rv_r)}{\partial r} + \frac{1}{r}\frac{\partial v_\theta}{\partial\theta} + \frac{\partial v_z}{\partial z} = 0 \tag{4}$$

$$\begin{aligned}
&v_r\frac{\partial v_r}{\partial r} + \frac{v_\theta}{r}\frac{\partial v_r}{\partial\theta} + v_z\frac{\partial v_r}{\partial z} - \frac{v_\theta^2}{r} = -\frac{\partial P_1}{\partial r}\\
&\quad + Pr\left(\frac{\partial^2 v_r}{\partial r^2} + \frac{1}{r}\frac{\partial v_r}{\partial r} + \frac{1}{r^2}\frac{\partial^2 v_r}{\partial\theta^2} - \frac{v_r}{r^2} - \frac{2}{r^2}\frac{\partial v_\theta}{\partial\theta}\right)\\
&\quad + Pr^2(Gr_{\mathrm{t}}T + Gr_{\mathrm{c}}C)\cos\theta\cos\alpha
\end{aligned} \tag{5a}$$

$$\begin{aligned}
&v_r\frac{\partial v_\theta}{\partial r} + \frac{v_\theta}{r}\frac{\partial v_\theta}{\partial\theta} + v_z\frac{\partial v_\theta}{\partial z} + \frac{v_r v_\theta}{r} = -\frac{\partial P_1}{r\partial\theta}\\
&\quad + Pr\left(\frac{\partial^2 v_\theta}{\partial r^2} + \frac{1}{r}\frac{\partial v_\theta}{\partial r} + \frac{1}{r^2}\frac{\partial^2 v_\theta}{\partial\theta^2} - \frac{v_\theta}{r^2} + \frac{2}{r^2}\frac{\partial v_r}{\partial\theta}\right)\\
&\quad - Pr^2(Gr_{\mathrm{t}}T + Gr_{\mathrm{c}}C)\sin\theta\cos\alpha
\end{aligned} \tag{5b}$$

$$\begin{aligned}
&v_r\frac{\partial v_z}{\partial r} + \frac{v_\theta}{r}\frac{\partial v_z}{\partial\theta} + v_z\frac{\partial v_z}{\partial z}\\
&\quad = -\frac{\mathrm{d}P_2}{\mathrm{d}z} + Pr\left(\frac{\partial^2 v_z}{\partial r^2} + \frac{1}{r}\frac{\partial v_z}{\partial r} + \frac{1}{r^2}\frac{\partial^2 v_z}{\partial\theta^2}\right)\\
&\qquad + \frac{Pr\sin\alpha}{Re}(Gr_{\mathrm{t}}T + Gr_{\mathrm{c}}C)
\end{aligned} \tag{5c}$$

$$v_r\frac{\partial T}{\partial r} + \frac{v_\theta}{r}\frac{\partial T}{\partial\theta} + v_z\frac{\partial T}{\partial z} = \frac{\partial^2 T}{\partial r^2} + \frac{1}{r}\frac{\partial T}{\partial r} + \frac{1}{r^2}\frac{\partial^2 T}{\partial\theta^2} \tag{6}$$

$$v_r\frac{\partial C}{\partial r} + \frac{v_\theta}{r}\frac{\partial C}{\partial\theta} + v_z\frac{\partial C}{\partial z} = Le\left(\frac{\partial^2 C}{\partial r^2} + \frac{1}{r}\frac{\partial C}{\partial r} + \frac{1}{r^2}\frac{\partial^2 C}{\partial\theta^2}\right) \tag{7}$$

These expressions of the governing equations show that the problem under study is characterised by six independent parameters: the Reynolds number, the Prandtl number, the Lewis number, the thermal Grashof number, the solutal Grashof number, and the inclination angle of the tube. Some authors [13] rewrite the terms $(Gr_{\mathrm{t}}T + Gr_{\mathrm{c}})$ as $Gr_{\mathrm{t}}(T + NC)$ where N indicates the buoyancy ratio $(N = Gr_{\mathrm{c}}/Gr_{\mathrm{t}})$. This formulation is not generalised and is not practical for flows in adiabatic tubes ($q = 0$ or $Gr_{\mathrm{t}} = 0$). Therefore it has not been used here. It should be noted that when $Gr_{\mathrm{t}} = Gr_{\mathrm{c}} = 0$ the velocity distribution is not influenced by either temperature or concentration gradients (forced convection). When $Gr_{\mathrm{t}} = 0$ and $Gr_{\mathrm{c}} \neq 0$ the velocity field is influenced by solutal buoyancy (mixed convection due to concentration gradients) and in turn perturbs the temperature

distribution. When $Gr_t \neq 0$ and $Gr_c = 0$ the velocity field is influenced by thermal buoyancy (mixed convection due to temperature gradients) and in turn perturbs the concentration distribution. Finally, when both $Gr_t \neq 0$ and $Gr_c \neq 0$ the velocity, temperature and concentration distributions are all coupled together (mixed convection due to both temperature and concentration gradients).

An additional constraint to be satisfied at every axial location is the overall mass balance, which is used to deduce the axial pressure gradient in the momentum equation (5c):

$$\int_0^{0.5}\int_0^{\pi} v_z r \,\mathrm{d}\theta \,\mathrm{d}r = \frac{\pi}{8} \tag{8}$$

The boundary conditions based on the assumptions of uniform entry and symmetry about the vertical diameter are:

$$^{*}\text{ at } z = 0 \qquad v_z = 1 \quad \text{and} \quad v_\theta = v_r = T = C = 0 \tag{9a}$$

$$^{*}\text{ at } \theta = 0, \pi \qquad v_\theta = \frac{\partial v_r}{\partial \theta} = \frac{\partial v_z}{\partial \theta} = \frac{\partial T}{\partial \theta} = \frac{\partial C}{\partial \theta} = 0 \tag{9b}$$

Finally, the condition at the fluid-solid interface is

$$^{*}\text{ at } r = 0.5 \qquad v_\theta = v_r = v_z = 0, \quad C = 1 \quad \text{and} \quad \frac{\partial T}{\partial r} = 1.0 \tag{9c}$$

Once the velocity, temperature and concentration fields have been calculated, the following quantities of practical interest are computed. The average wall shear stress which is expressed as:

$$\tau_z = \frac{1}{\pi}\int_0^{\pi} \left.\frac{\partial v_z}{\partial r}\right|_{r=0.5} \mathrm{d}\theta \tag{10a}$$

the average Nusselt number which is given by:

$$Nu_z = \frac{1}{\overline{T}_w - T_b} \tag{10b}$$

where

$$\overline{T}_w = \frac{1}{\pi}\int_0^{\pi} T_w \,\mathrm{d}\theta \quad \text{and} \quad T_b = \frac{8}{\pi}\int_0^{0.5}\int_0^{\pi} v_z T r \,\mathrm{d}\theta \,\mathrm{d}r$$

and the average Sherwood number which is defined as:

$$Sh_z = \overline{\left(\frac{\partial C}{\partial r}\right)}_{r=0.5}\left(\frac{1}{1 - C_b}\right) \tag{10c}$$

where

$$\overline{\left(\frac{\partial C}{\partial r}\right)}_{r=0.5} = \frac{1}{\pi}\int_0^{\pi}\left(\frac{\partial C}{\partial r}\right)_{r=0.5} \mathrm{d}\theta \quad \text{and}$$

$$C_b = \frac{8}{\pi}\int_0^{0.5}\int_0^{\pi} v_z C r \,\mathrm{d}\theta \,\mathrm{d}r$$

3. Solution method

The set of coupled non-linear equations was solved numerically using a version of the Patankar–Spalding [18] method for three-dimensional axially parabolic flows. A marching technique based on the SIMPLEC algorithm for handling the in-plane pressure velocity coupling [19], the power law scheme for the approximation of the in-plane convective-diffusive terms, and the procedure proposed by Raithby and Schneider [20] for the calculation of the axial pressure gradient were used.

For enhanced accuracy, grids were chosen to be uniform in the circumferential direction but non-uniform in the radial and axial directions to account for the uneven variations of velocity, temperature and concentration near the tube wall and in the entrance region. Numerical experiments were performed to ensure grid independence of the numerical results. Table 1 gives a comparison of local Nusselt and Sherwood numbers for five different grid arrangements. These grids are defined by two numbers indicating the number of nodes in the circumferential and radial directions respectively and by an alphanumeric combination describing the axial grid distribution. The latter is defined in Table 2, which indicates the distance between successive

Table 1
Comparison of Nusselt and Sherwood numbers for various grid arrangements and $Gr_t = Gr_c = 1.01 \times 10^5$, $Le = 1$, $Pr = 0.7$ and $\alpha = 0°$

Z	10^{-4}	1.01×10^{-3}	5.01×10^{-3}	1.2×10^{-1}
$26 \times 22 - D_1$				
Nu_z	62.77	17.42	9.07	6.30
Sh_z	44.12	12.64	6.92	5.77
$36 \times 32 - D_1$				
Nu_z	51.03	17.3	9.04	6.29
Sh_z	36.43	12.69	6.93	5.78
$46 \times 42 - D_1$				
Nu_z	49.86	17.26	9.04	6.27
Sh_z	35.67	12.73	6.94	5.77
$36 \times 32 - D_2$				
Nu_z	51.43	17.36	9.06	6.27
Sh_z	36.78	12.71	6.94	5.76
$36 \times 32 - D_3$				
Nu_z	44.5	17.23	9.10	6.27
Sh_z	33.9	12.90	7.05	5.76

Table 2
Characteristics of the axial grid distributions

D_1		D_2		D_3	
Δz	I_z	Δz	I_z	Δz	I_z
10^{-6}	1–9	10^{-6}	1–19	10^{-6}	1–9
10^{-5}	10–19	10^{-5}	20–49	5×10^{-5}	10–19
10^{-4}	20–79	10^{-4}	50–149	5×10^{-4}	20–79
5×10^{-4}	80–119	5×10^{-4}	150–249	10^{-3}	80–119
10^{-3}	120–149	10^{-3}	250–	2×10^{-3}	120–149
2×10^{-3}	150–			4×10^{-3}	150–

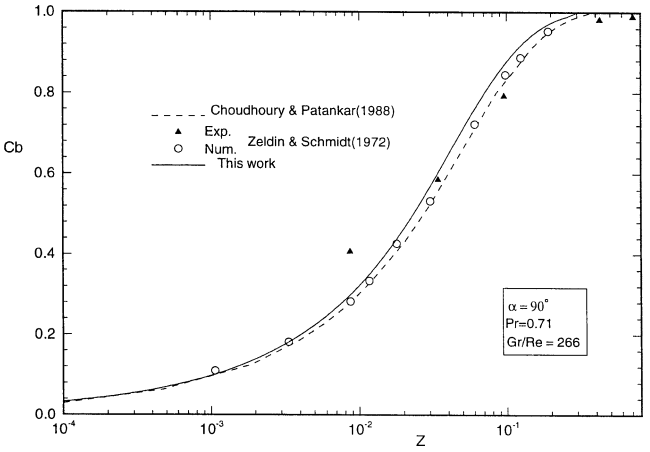

Fig. 2. Validation for mixed convection in an isothermal tube.

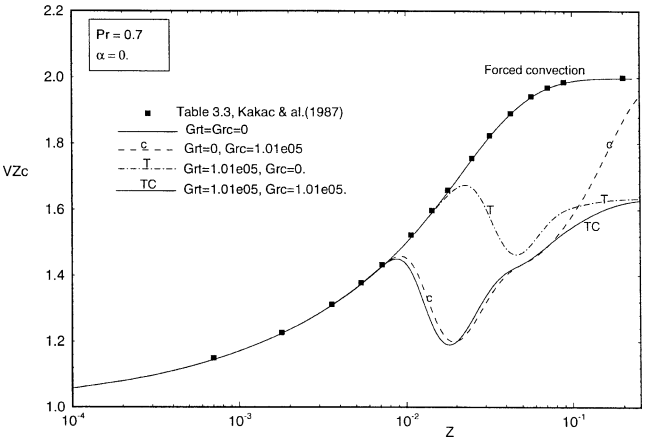

Fig. 3. Evolution of the centreline axial velocity in a horizontal tube.

cross sections. Thus for D_1 the axial distance is 10^{-6} between the first ten cross sections, etc. The results of Table 1 show that the differences in Nu_z and Sh_z computed using the $36 \times 32 - D_1$, $46 \times 42 - D_1$ or $36 \times 32 - D_2$ grids are always very small (within 1% for $z \geqslant 1.01 \times 10^{-3}$). Thus the grid $36 \times 32 - D_1$ is adequate for the calculations presented in this paper.

To check the validity of the model and the precision of the numerical scheme, the developing flow, thermal and concentration fields were computed for $Le = 1$ without buoyancy effects ($Gr_t = Gr_c = 0$) and were compared with the results for forced convection found in the literature. Because of the selected interfacial boundary conditions (9c) the calculated temperature profile corresponds to the published temperature distribution in a tube with uniform interfacial heat flux while the calculated concentration corresponds to the temperature distribution in an isothermal tube. Both these comparisons showed excellent agreement between our results and those published by Kays and Crawford [21]. Furthermore, we compared the velocity and temperature fields for $Gr_t \neq 0$ and $Gr_c = 0$ with corresponding results for thermally induced mixed convection in uniformly heated tubes by Orfi et al. [7] and obtained, once again, excellent agreement. Finally, we calculated the velocity and concentration fields in a vertical tube for $Gr_t = 0$, $Gr_c \neq 0$ and $Le = 1$. As explained earlier, this concentration field corresponds to the developing temperature field for mixed convection in an isothermal tube. Comparisons of our calculated results with corresponding experimental and numerical results by Zeldin and Schmidt [22] and by Choudhury and Patankar [5] show very good agreement (see Figs. 2 and 3 for some of these comparisons in the cases of mixed and forced convection, respectively).

All these tests confirm that the proposed model and the adopted solution procedure are suitable for the present study of the simultaneously developing velocity, temperature and concentration fields inside circular tubes.

4. Results and discussion

In the following presentation a detailed description of mixed convection with heat and mass transfer inside horizontal and vertical tubes is provided in terms of velocity, temperature and concentration profiles, thermal and concentration contours as well as axial distributions of the Nusselt number, the Sherwood number and the wall shear stress. The Reynolds, Prandtl and Lewis numbers are fixed at 400, 0.7 and 1, respectively. Four different combinations of buoyancy parameters (thermal and solutal Grashof numbers) have been considered:

(i) $Gr_t = Gr_c = 0$,
(ii) $Gr_t = 0$, $Gr_c = 1.01 \times 10^5$,
(iii) $Gr_t = 1.01 \times 10^5$, $Gr_c = 0$,
(iv) $Gr_t = Gr_c = 1.01 \times 10^5$.

The first of these combinations corresponding to pure forced convection serves as the reference for the evaluation of natural convection effects. The next two, with one of the Grashof numbers equal to zero, show the effects of thermal or solutal buoyancy acting alone. The fourth case illustrates the combined effects of both mechanisms.

4.1. Case of horizontal tubes

Fig. 3 shows the evolution of the centreline axial velocity V_{zc} for a horizontal orientation of the tube ($\alpha = 0°$, see Fig. 1). It is seen that close to the inlet natural convection has no effect. For case (ii), identified by the letter C in the figure, the effects of solutal buoyancy manifest themselves from $z \cong 8 \times 10^{-3}$: the centreline axial velocity decreases and goes through a local minimum at $z \cong 0.02$. For case (iii), identified by the letter T in the figure, thermal buoyancy acting alone has a similar effect but the minimum value occurs later (at $z \cong 0.05$). It should be noted that such a local minimum has been observed experimentally by Zeldin

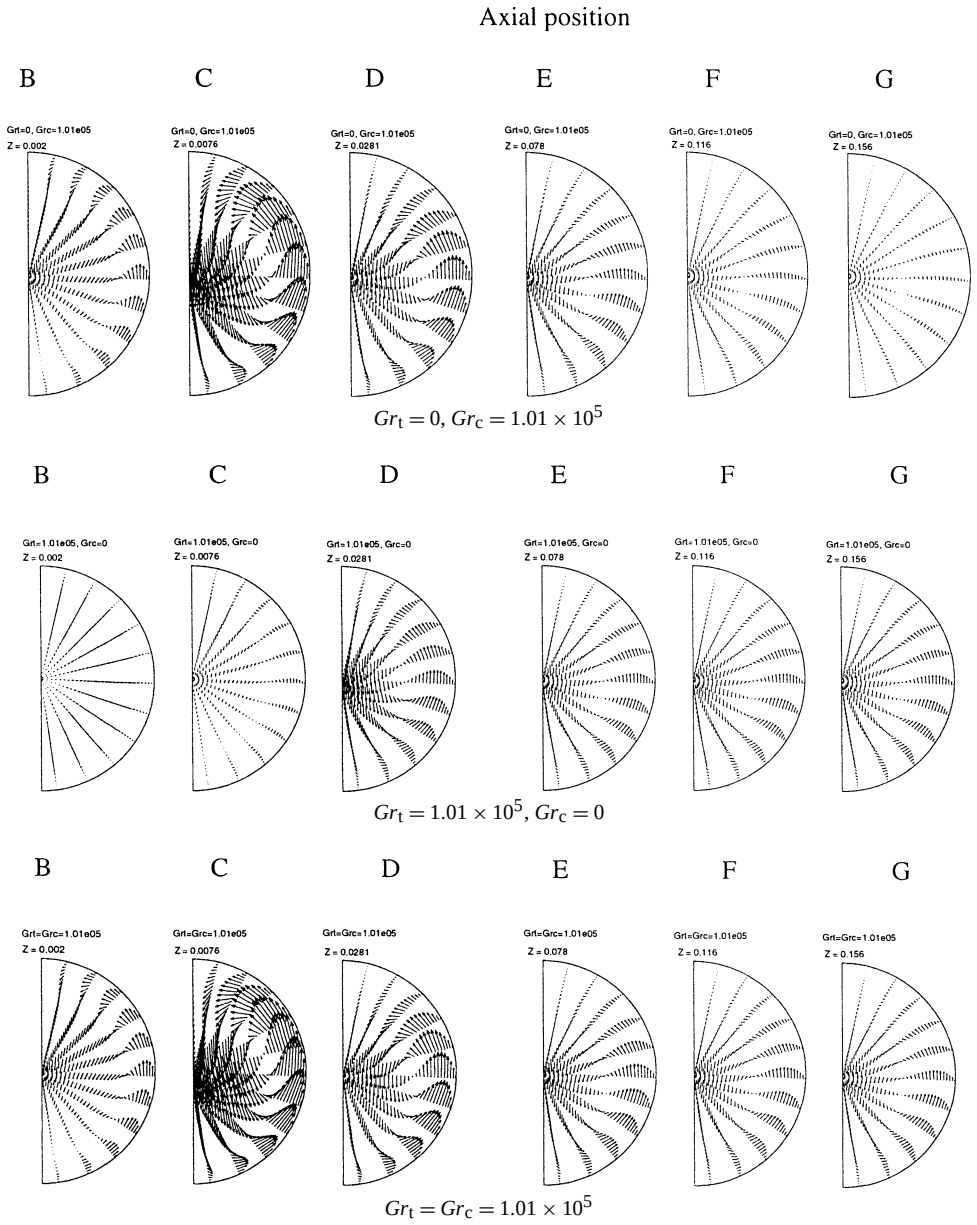

Fig. 4. Evolution of the secondary flow in a horizontal tube.

and Schmidt [22] for the case of mixed convection in an isothermal vertical pipe. A significant difference between cases (ii) and (iii) concerns the behaviour of this axial velocity near the tube outlet: when solutal buoyancy acts alone V_{zc} approaches the value 2 (corresponding to pure forced convection) whereas in the case with only thermal buoyancy it approaches the value 1.64. The behaviour of the centreline velocity for case (iv) with combined thermal and solutal buoyancies (identified by the letters TC in the figure) can be examined by distinguishing four separate regions. For $z \leqslant 8 \times 10^{-3}$ its evolution is identical to the corresponding one for forced convection indicating that natural convection is very weak. For $8 \times 10^{-3} \leqslant z \leqslant 0.08$ the centreline velocity for case (iv) is essentially the same as that for case (ii) indicating that solutal buoyancy predominates. For values of z between approximately 0.08 and 0.5 the centreline velocity for case (iv) seems to be influenced by both the solutal and thermal buoyancy forces while beyond $z = 0.5$ this velocity is essentially the same as that for case (iii) indicating that thermal buoyancy predominates.

To further illustrate the effects of thermal and/or solutal buoyancy forces we present in Fig. 4 the buoyancy induced secondary flow for cases (ii), (iii) and (iv) at six different cross sections B, C, D, E, F and G of the tube situated at $z =$ 0.002, 0.0076, 0.0281, 0.078, 0.116 and 0.156, respectively. At the first axial location, $z = 0.002$, the secondary flow field for case (ii) is already affected by the solutal buoyancy force. One can observe an upward flow confined in a thin layer near the wall and a downward flow along the vertical diameter. At this same axial location, the secondary velocities for case

(iii) are essentially radial indicating that thermal buoyancy has not yet had any effect and that boundary layer growth is the only phenomenon present. For the same axial location, the flow field for case (iv) with both heat and mass transfer influencing the velocity field is essentially the same as the corresponding one for case (ii). This is consistent with the previous remarks regarding cases (ii) and (iii). As the fluid moves downstream, the buoyancy forces are in effect for all three cases. Initially, the strength of the secondary swirling flow increases and becomes most intense at cross section C for cases (ii) and (iv) and at cross section D for case (iii). In all cases the centre of circulation moves away from the wall as the fluid moves along the tube. Further downstream, the secondary flow becomes weaker and reaches different fully developed states. Thus for case (ii) we notice that at cross section G the effects of solutal buoyancy have almost disappeared and the swirling secondary motion is negligible. On the other hand, for cases (iii) and (iv) the effects of thermal buoyancy are never attenuated since the continuous heating of the fluid maintains significant temperature gradients in all cross sections.

The observations regarding the axial development of the primary (Fig. 3) and secondary (Fig. 4) flow fields can be explained by examining the concentration and temperature fields illustrated in Figs. 5 and 6, respectively. In the vicinity of the tube entrance (section C at $z = 0.0076$) most of the fluid is still at a temperature and concentration close to those of the inlet. Therefore, up to this cross section, the evolution of the centreline axial velocity (Fig. 2) is only due to the growth of the boundary layer along the wall. Thus it is exactly the same for the three mixed convection cases and for the forced convection case. Furthermore, it is noted that, at this early cross section, the isotherms and iso-concentration lines for $Gr_c = 0$ are essentially circular. This situation implies that the circumferential gradients are very small and that, therefore, the in-plane induced motion is extremely weak as observed in the corresponding part of Fig. 4. On the other hand, for $Gr_c \neq 0$ the isotherms and iso-concentration lines are not circular and the ensuing circumferential gradients give rise to the intense secondary flow shown in the corresponding parts of Fig. 4.

At $z = 0.0281$ (cross section D) the shape of the isotherms and iso-concentration lines is severely distorted from the earlier circular pattern. The flattened shape of these lines in the upper half of the tube generates important circumferential gradients which cause the high intensity secondary flow illustrated in Fig. 4. In the lower half of the tube where these lines are still nearly circular the secondary flow is indeed weaker. It should also be noted that the distortion of these lines is much more severe when $Gr_c \neq 0$ and that, as a consequence, the corresponding swirling motion is considerably stronger than when $Gr_c = 0$ (cf., Fig. 4). Finally, it must be pointed out that the temperature and concentration throughout this cross section are different from the corresponding entrance values (this point is further documented in Fig. 8).

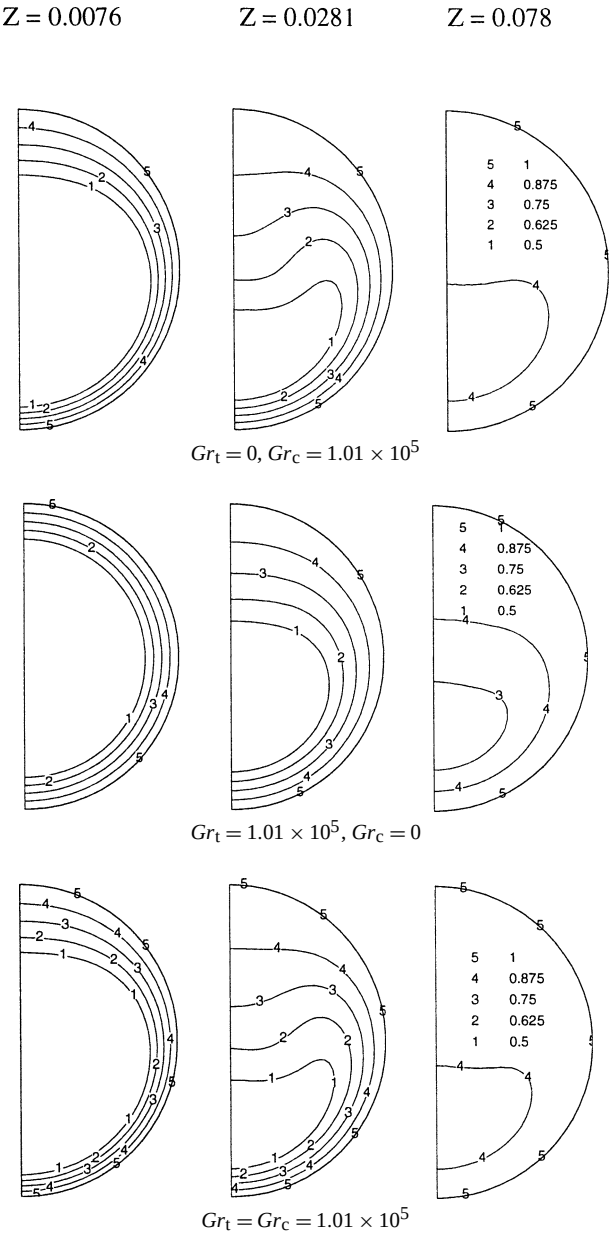

Fig. 5. Concentration distribution in a horizontal tube.

As a result, the centreline axial velocity is no longer the same as for forced convection (cf., Fig. 3).

Further away from the entrance (cross section E at $z = 0.078$), and in accordance with the prescribed boundary conditions, the concentration in all cases tends to become uniform and equal to unity ($C \to 1$ as z increases) whereas the temperature tends towards a non-uniform distribution which is identical for the two cases with $Gr_t \neq 0$ (see Fig. 7). These results indicate that the effects of solutal buoyancy disappear as $z \to \infty$ and, therefore, the axial velocity profile for case (ii) tends towards the parabolic forced convection velocity distribution. This tendency is clearly observed in Fig. 3 ($V_{zc} \to 2$ as $z \to \infty$) and 8. On the other hand, in case (iii) the effects of thermal buoyancy are never attenuated since the continuous heating of the

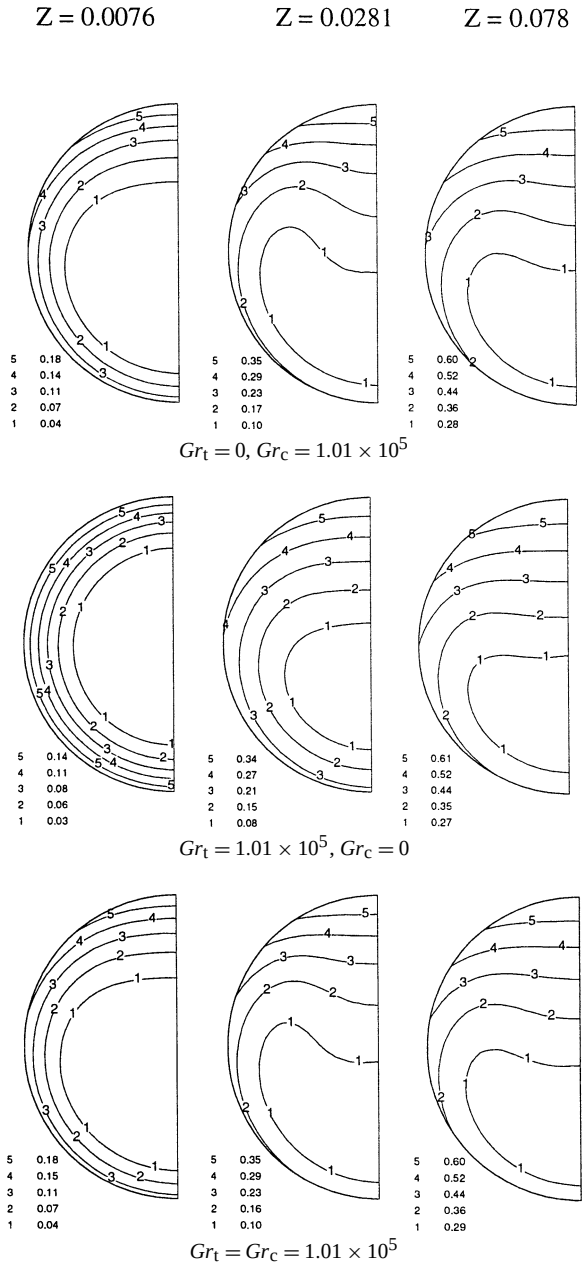

Fig. 6. Axial evolution of isotherms in a horizontal tube.

fluid maintains significant temperature gradients in all cross sections.

The evolution of the axial velocity, concentration and temperature profiles along the vertical symmetry line are shown in Fig. 8 for cases (ii) and (iii). The corresponding results for case (iv) are essentially identical to those for case (ii) up to approximately $z = 0.08$ and approach asymptotically those of case (iii) as z increases beyond this position. For any given radial position, the concentration and temperature increase monotonically with z while the axial velocity shows a more complex behaviour as exemplified by Fig. 3. Very close to the tube entrance the profiles are unaffected by buoyancy: all three variables are uniform in the central part of the tube and their distribution is symmetrical with respect

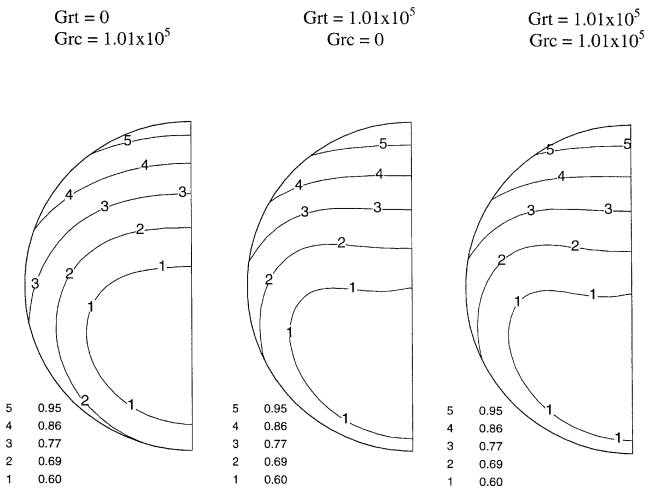

Fig. 7. Temperature distribution at $z = 0.156$ for a horizontal tube.

to the tube axis. Further downstream (section D) the effects of buoyancy become evident as the uniform portion and the symmetry disappear. The maximum velocity, minimum concentration and minimum temperature occur below the tube axis similarly to the result reported by Yan [13] for a rectangular duct. The maximum velocity is higher for $Gr_t \neq 0$ indicating that the effect of thermal buoyancy on the velocity is more important than that of solutal buoyancy. The minimum concentration is higher for $Gr_c \neq 0$ as expected but, surprisingly, the minimum temperature is essentially the same for both $Gr_c \neq 0$ and $Gr_t \neq 0$. Even further downstream (sections E and beyond) the concentration for $Gr_c \neq 0$ is uniformly higher than the corresponding value for $Gr_t \neq 0$. As noted earlier it tends towards unity for both cases. As this limiting value is approached, the solutal buoyancy force becomes negligible and the flow field for $Gr_t = 0$ tends towards the fully developed forced convection solution: the axial velocity profile becomes axisymetric and parabolic while the isotherms within a cross section become circular with their center at the tube axis. Similarly, when $Gr_t \neq 0$, as $z \to \infty$ and $C \to 1$ the flow field tends towards the fully developed mixed convection solution in a uniformly heated tube [7].

The influence of the temperature and/or concentration gradients on the average values of the wall shear stress and of the Nusselt, Sherwood numbers is presented in Fig. 9. The excellent agreement of our results for forced convection with those of Kays and Crawford [21] provides further evidence of the validity of our model and numerical procedure. The results shown in this figure confirm that the influence of buoyancy is negligible close to the tube inlet. The axial position where these effects become noticeable, i.e., where the values of these three quantities are no longer identical to those for forced convection, depends on the relative importance of the two Grashof numbers. Thus it is approximately equal to 4×10^{-3} for cases (ii) and (iv) with $Gr_c \neq 0$ while for case (iii) with $Gr_c = 0$ it is approximately 1.5×10^{-2}. These results are consistent with those of the previous figures, which show that the effects

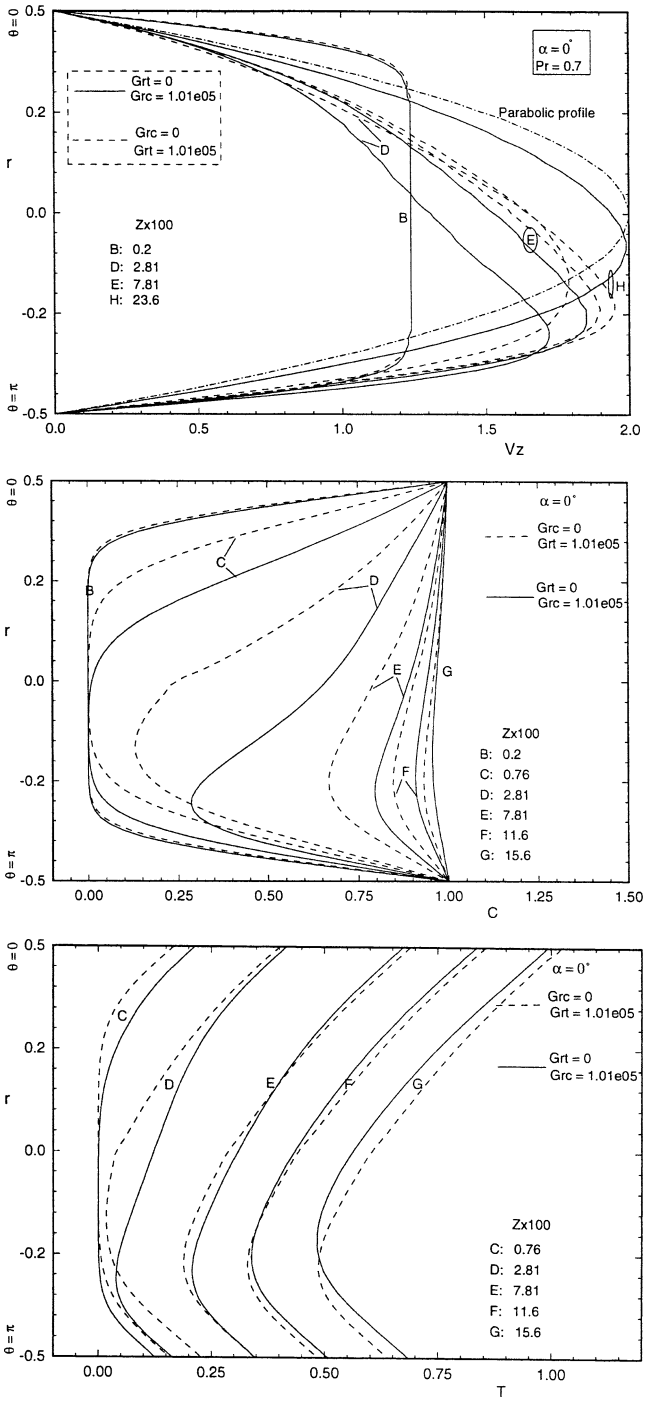

Fig. 8. Evolution of axial velocity, concentration and temperature profiles along the vertical diameter of a horizontal tube.

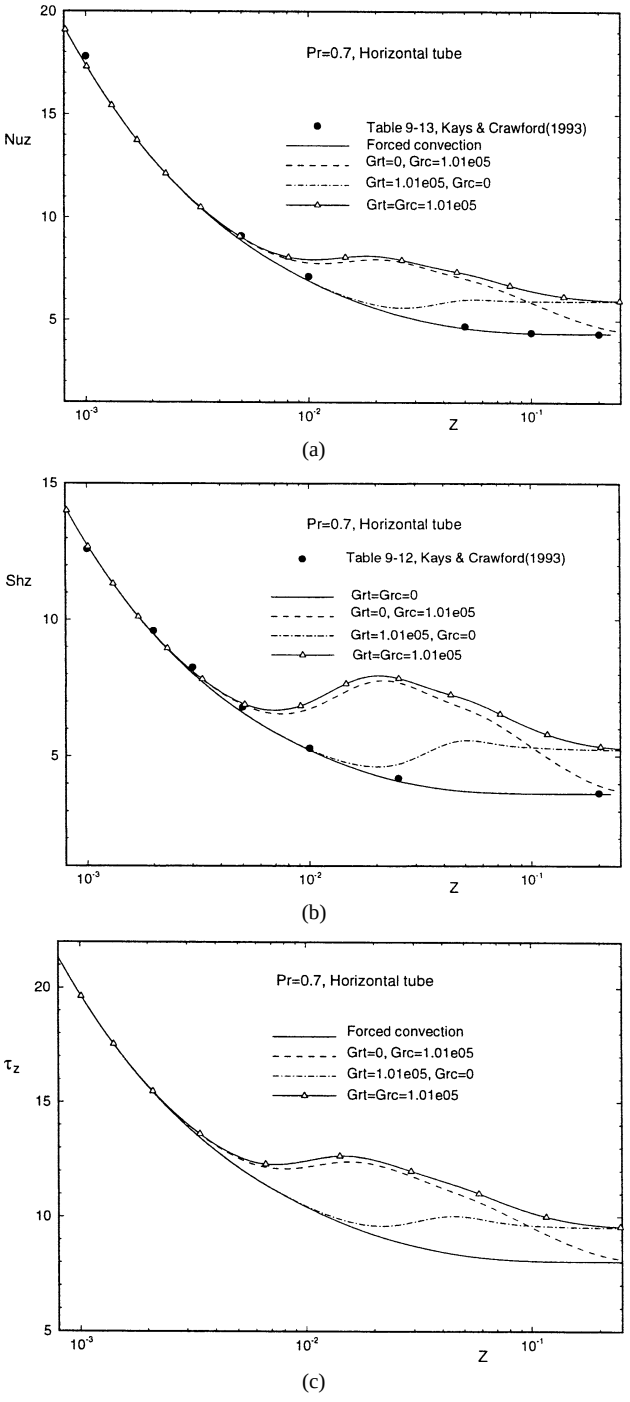

Fig. 9. Axial variation of the wall shear stress and of the Nusselt, Sherwood numbers in a horizontal tube.

of solutal buoyancy become evident much earlier than those of thermal origin. Beyond these positions τ_z, Nu_z and Sh_z are significantly different from the corresponding values for forced convection. The vigorous growth of the secondary flow observed in Fig. 4 results in an increase of the flow resistance and of the rates of heat and mass transfer. The three quantities τ_z, Nu_z and Sh_z attain a local maximum and then decrease towards different fully developed states. It is important to mention that the local maxima of Nu_z, Sh_z and τ_z occur at the locations where the buoyancy effects are the strongest. This takes place at approximately 2×10^{-3} for cases (ii) and (iv) and at $z \cong 5 \times 10^{-2}$ for case (iii). One can also note that in the intermediate region, between the essentially forced convection and the fully developed regions, the enhancement in heat, mass transfer and flow resistance is more important for the cases with $Gr_c \neq 0$ than for the case with $Gr_c = 0$. Finally, it is noted that the fully developed values for all three quantities are identical for

cases (iii) and (iv) for which $Gr_t \neq 0$ and are significantly higher than those for case (ii) with $Gr_t = 0$. In accordance with previous remarks, the latter values are identical with the corresponding ones for forced convection.

4.2. Case of vertical tubes

In this section results for a vertical tube are presented and discussed. It must be noted that for this tube inclination there is no secondary in-plane flow such as the one shown in Fig. 4 since the buoyancy forces always act upwards, i.e., parallel to the flow direction. On the other hand, depending on whether the flow is upward or downward, these forces respectively aid or oppose the movement of the fluid. The effect of the relative importance of the Grashof numbers is investigated for both upflow (aiding buoyancy) and downflow (opposing buoyancy) situations. In the case of opposing buoyancy, flow reversal may occur [23] but such conditions were not considered because of the limitations of the axially parabolic model employed in this study.

Fig. 10 clearly illustrates the dependence of the centreline velocity on the values of the two Grashof numbers as well as on the direction of flow. We observe two very different behaviours for this velocity: for upward flow it is smaller than the corresponding velocity for forced convection while for downward flow it is greater than this reference case. This situation prevails throughout the length of the tube except in the entrance region ($z < 3 \times 10^{-4}$) where the centreline velocity for all cases is essentially the same. For case (ii) for which $Gr_c = 1.01 \times 10^5$, $Gr_t = 0$ and for upward flow, the centreline velocity initially increases but less rapidly than the corresponding one for forced convection. It reaches a local maximum at $z \cong 5 \times 10^{-3}$ and then decreases dramatically until it reaches a minimum value of about 0.65 at $z \cong 3.5 \times 10^{-2}$. This behaviour has been observed experimentally by Zeldin and Shmidt [22] for the equivalent problem of upward mixed convection in an isothermal vertical tube. On the other hand, for downward flow V_{zc} increases more rapidly than the corresponding one for forced convection towards a maximum value approximately equal

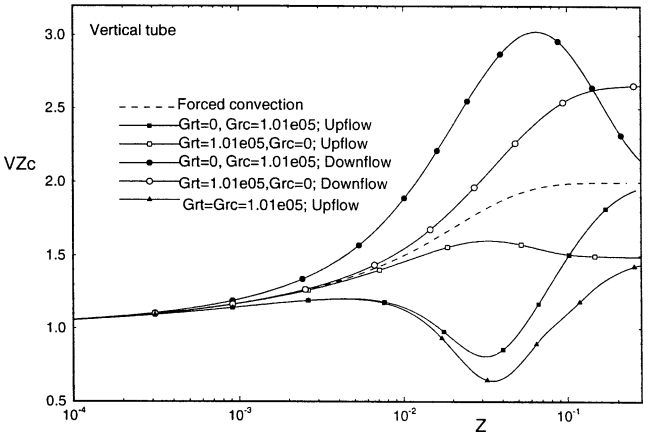

Fig. 10. Evolution of the centreline axial velocity in a vertical tube.

to 3 at $z \cong 6 \times 10^{-2}$. After these particular locations, as z increases, V_{zc} tends towards 2, the corresponding value for forced convection. For case (iii) for which $Gr_t = 1.01 \times 10^5$, $Gr_c = 0$, the effect of thermal buoyancy force persists in the fully developed region. Thus, for upward flow this velocity reaches a maximum of approximately 1.6 at $z \cong 3 \times 10^{-2}$ and then decreases towards an asymptotic value approximately equal to 1.5. For downward flow it increases monotonically towards an asymptotic value approximately equal to 2.7. Finally, for case (iv) with $Gr_t = Gr_c = 1.01 \times 10^5$ and upward flow, the centreline velocity is initially influenced only by solutal buoyancy and is therefore almost identical to that for case (ii). Further downstream, thermal buoyancy becomes effective and as z increases the velocity tends towards the same asymptotic value as for case (iii). This is of course due to the fact that, as $z \to \infty$, the concentration becomes uniform and solutal buoyancy disappears.

Fig. 11 shows the development of the axial velocity profile for different conditions. For upward flow, the fluid near the tube wall is accelerated by the buoyancy force and its velocity is greater than the corresponding one for forced convection. In the core region the opposite is true as a consequence of mass conservation. This relationship between the velocities for mixed and forced convection is valid for both cases (ii) and (iii). The difference from the forced convection profile is most pronounced for case (ii) with $Gr_t = 0$ at cross section D where the maximum velocity does not occur at the centreline. For larger values of Gr_c, flow reversal will occur close to the axis as is the case for thermally induced upward mixed convection with large values of Gr_t [6,23]. For downward mixed convection, the upwards acting buoyancy forces decelerate the fluid near the wall with a corresponding increase of velocity near the centreline. At large values of the Grashof numbers, flow reversal will occur in the vicinity of the wall. It should also be noted that for case (ii) with $Gr_t = 0$, $Gr_c \neq 0$, as $z \to \infty$ the velocity profile tends towards the parabolic profile of forced convection for both upward and downward flow. On the other hand, for case (iii) with $Gr_t \neq 0$, $Gr_c = 0$ the velocity profile tends towards a fully developed state which is quite different from the corresponding forced convection profile.

The wall shear stress axial evolution is presented in Fig. 12 for both upflow and downflow convection. For forced flow ($Gr_c = Gr_t = 0$), which is shown as a reference, it approaches the asymptotic value of 8 in the fully developed region. Two different behaviours are observed for mixed convection. For upflow, since the fluid near the wall accelerates (Fig. 11), the wall shear stress is higher than the corresponding one for forced convection. For downflow, it is smaller than that of forced convection due to the deceleration occurring near the tube wall (Fig. 11). In this case, it is noted that the wall shear stress approaches zero when the solutal buoyancy force acts alone ($Gr_c = 1.01 \times 10^5$, $Gr_t = 0$) indicating that flow reversal can occur in the vicinity of the wall. Far

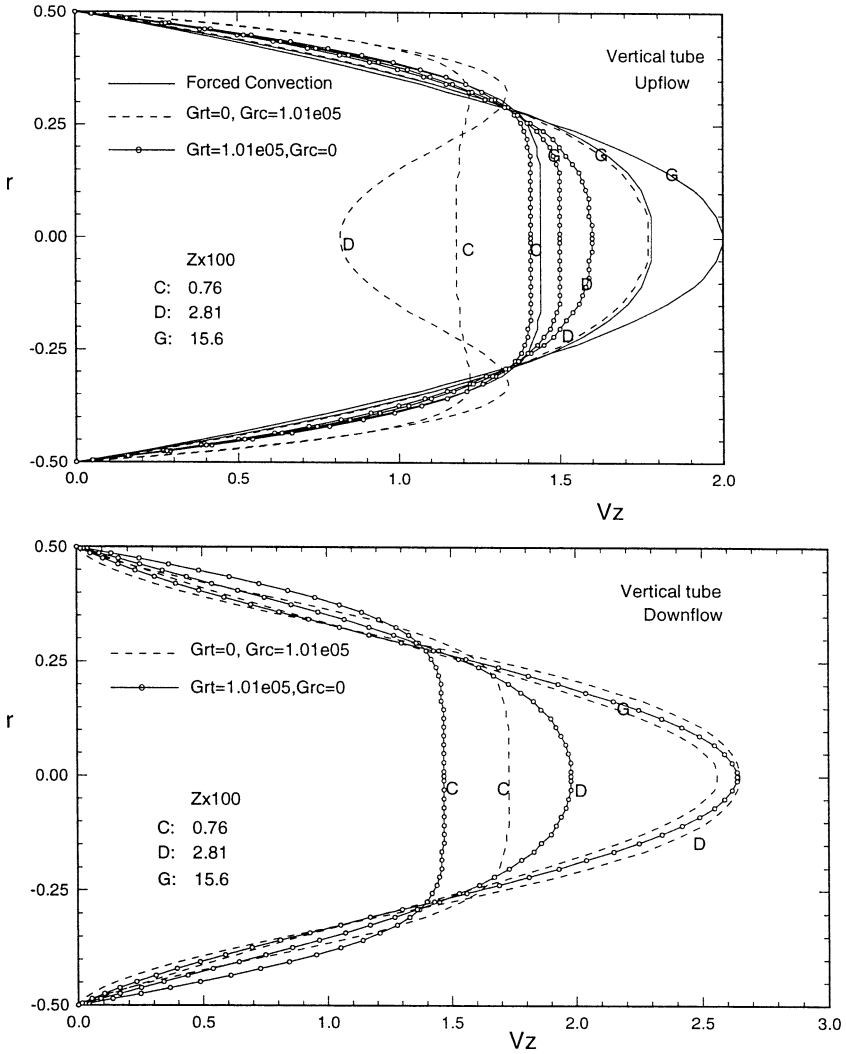

Fig. 11. Evolution of the axial velocity profile in a vertical tube.

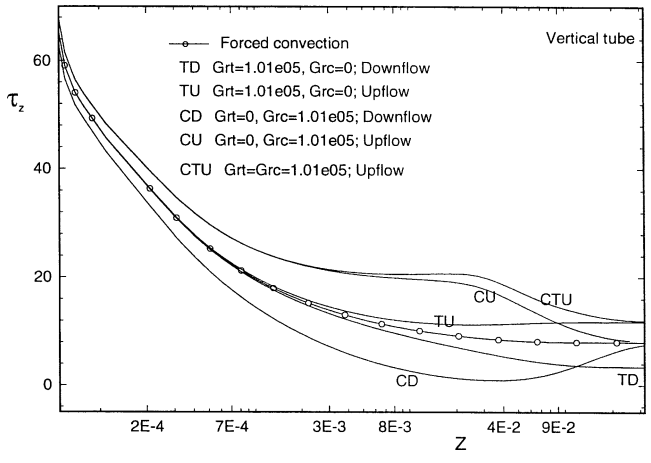

Fig. 12. Axial variation of the wall shear stress in a vertical tube.

downstream, the wall shear stress tends to different asymptotic values which are independent of the solutal Grashof number. They depend on the value of the thermal Grashof number as well as on the direction of flow and are different from the corresponding ones for the horizontal tube.

Finally, Fig. 13 illustrates the axial distribution of the heat and mass transfer coefficients. The effects of the buoyancy forces on Nu_z and Sh_z are similar. Thus, for upflow the Nusselt and Sherwood numbers are higher than the corresponding values for forced convection ($Gr_c = Gr_t = 0$). For downflow, the opposite is true. These observations are valid throughout the length of the tube when $Gr_t \neq 0$. On the other hand, for $Gr_t = 0$ the assymptotic values of Nu_z and Sh_z are identical to those of forced convection for the reasons presented earlier. The assymptotic values for $Gr_t \neq 0$ depend on the value of this Grashof number as well as on the direction of flow and are independent of Gr_c.

5. Conclusion

The flow field for developing laminar mixed convection in tubes with uniform heat flux and concentration at the fluid-solid interface can be separated in four regions:

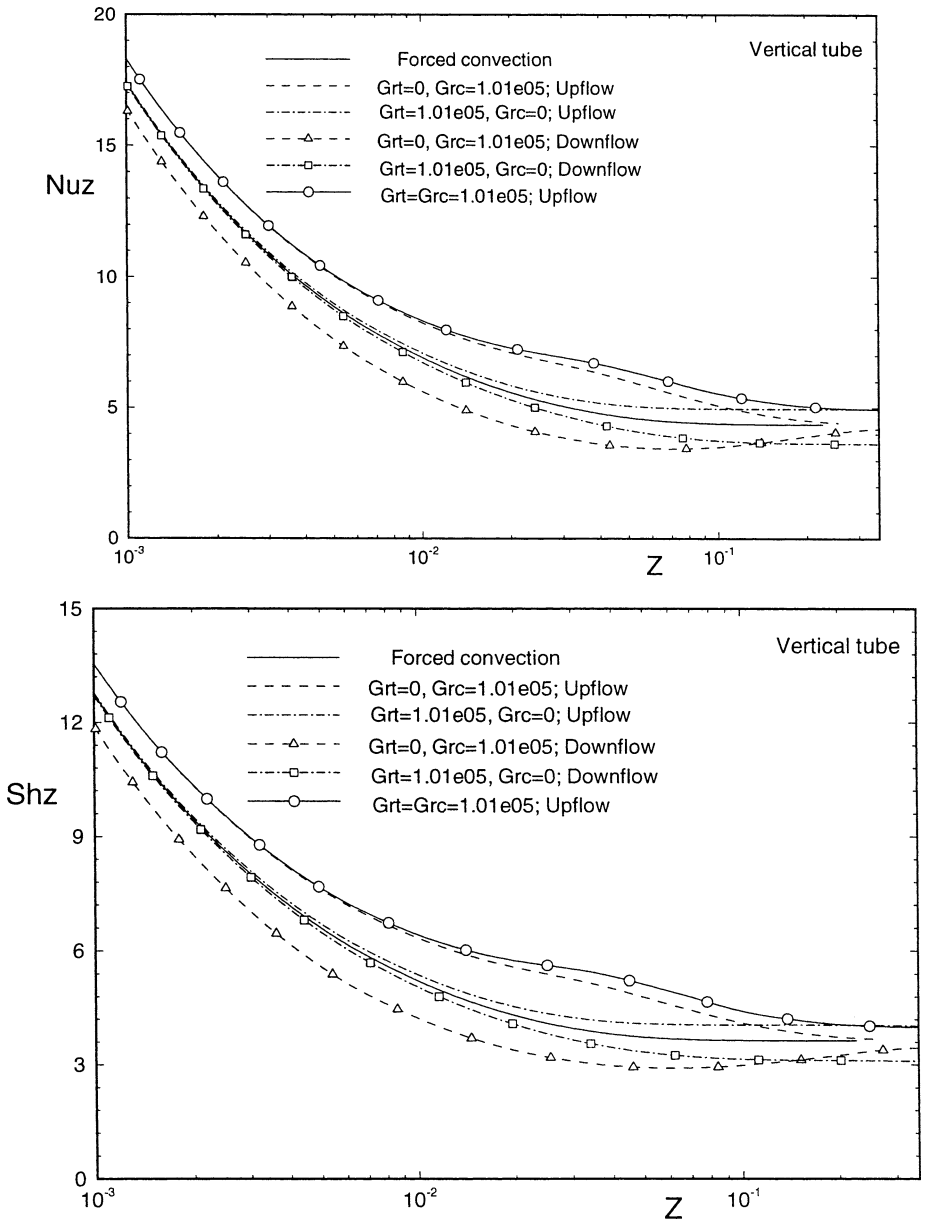

Fig. 13. Axial variation of the Nusselt and Sherwood numbers in a vertical tube.

(A) Very close to the tube inlet forced convection boundary layer development dominates. Accordingly, in this short entry region the wall shear stress as well as the Nusselt and Sherwood numbers decrease rapidly in the axial direction.

(B) Further downstream, the effects of solutal buoyancy predominate. In this region the values of τ_z, Nu_z and Sh_z depend on the solutal Grashof number and on the tube inclination.

(C) Further downstream, the flow field is influenced by both solutal and thermal buoyancy forces. The values of τ_z, Nu_z and Sh_z depend on both Grashof numbers and on the tube inclination.

(D) Far downstream, thermal effects predominate and eventually determine the fully dependent conditions. In this region the values of τ_z, Nu_z and Sh_z depend on the thermal Grashof number and on the tube inclination.

In the case of horizontal tubes, the values of τ_z, Nu_z and Sh_z are generally larger than the corresponding values for forced convection. In the case of vertical tubes, the flow field in the three regions where mixed convection effects are present (regions B, C and D) is also influenced by the relative direction of the flow and the predominant buoyancy force. Thus, for opposing buoyancy the values of τ_z, Nu_z and Sh_z are generally smaller than the corresponding values for forced convection. The opposite is true for aiding buoyancy.

Acknowledgements

The authors thank the "Faculté des Sciences de Monastir", the "Laboratoire d'Études des Systèmes Thermiques et Énergétiques de l'École Nationale d'Ingénieurs de Monastir" and the Natural Sciences and Engineering Research Council of Canada for their financial support.

References

[1] Y. Mori, K. Futagami, Forced convective heat transfer in uniformly heated horizontal tubes, 2nd report, theoretical study, Internat. J. Heat Mass Transfer 10 (1967) 1801–1813.
[2] B.S. Petukhov, A.F. Polyakov, Experimental investigation of viscogravitational fluid flow in a horizontal tube, Sci. Res. Inst. High Temp., translated from, Teplofizika Vysokikh Temperatur 5 (1) (1967) 87–95.
[3] G.S. Barozzi, E. Zankhini, M. Mariotti, Experimental investigation of combined free and forced convection in horizontal and inclined tubes, Meccanica 20 (1) (1985) 18–27.
[4] B.R. Morton, D.B. Ingham, D.J. Keen, P.J. Heggs, Recirculating combined convection in laminar pipe flow, ASME Trans. J. Heat Transfer 111 (1989) 107–113.
[5] D. Choudhury, S.V. Patankar, Combined forced and free laminar convection in the entrance region of an inclined isothermal tube, ASME Trans. J. Heat Transfer 110 (1988) 901–908.
[6] M. Wang, T. Tsuji, Y. Nagano, Mixed convection with flow reversal in the thermal entrance region of horizontal and vertical pipes, Internat. J. Heat Mass Transfer 37 (15) (1994) 2305–2319.
[7] J. Orfi, N. Galanis, C.T. Nguyen, Laminar mixed convection in the entrance region of inclined pipes with high uniform heat fluxes, ASHRAE Trans. 4221 (1998) 417–428.
[8] S. Kakac, R.K. Shah, W. Aung, Handbook of Single-Phase Convective Heat Transfer, Wiley, New York, 1987.
[9] B. Gebhart, L. Pera, The nature of vertical natural convection flows resulting from the combined buoyancy effects of thermal and mass diffusion, Internat. J. Heat Mass Transfer 14 (1971) 2025–2050.
[10] T.S. Chen, C.F. Yuh, Combined heat and mass transfer in natural convection along a vertical cylinder, Internat. J. Heat Mass Transfer 23 (1980) 451–461.
[11] T.F. Lin, C.J. Chang, M.W. Yan, Analysis of combined buoyancy effects of thermal and mass diffusion on laminar forced convection heat transfer in a vertical tube, ASME Trans. J. Heat Transfer 110 (1988) 337–344.
[12] K.T. Lee, H.L. Tsai, M.W. Yan, Mixed convection heat and mass transfer in vertical rectangular ducts, Internat. J. Heat Mass Transfer 40 (7) (1997) 1621–1631.
[13] M.W. Yan, Transport phenomena of developing laminar mixed convection heat and mass transfer in inclined rectangular ducts, Internat. J. Heat Mass Transfer 38 (15) (1995) 2905–2914.
[14] J.N. Lin, F.C. Chou, M.W. Yan, P.Y. Tzeng, Combined buoyancy effects of thermal and mass diffusion on laminar forced convection in the thermal entrance region of horizontal square channels, Canad. J. Chem. Engrg. 70 (1992) 681–689.
[15] K.T. Lee, M.W. Yan, Mixed convection heat and mass transfer in radially rotating rectangular ducts, Numer. Heat Transfer A 34 (1998) 747–767.
[16] J. Orfi, N. Galanis, S. Ben Nasrallah, Buoyancy effects of heat and mass transfer in developing laminar flow in a horizontal pipe, in: B. Sundun, C.A. Brebbia (Eds.), Adv. Computational Methods in Heat Transfer VI, WIT Press, 2000, pp. 363–372.
[17] B. Gebhart et al., Buoyancy Induced Flows and Transport, Hemisphere, New York, 1988, p. 971.
[18] S.V. Patankar, D.B. Spalding, A calculation procedure for heat, mass and momentum transfer in three-dimensional parabolic flow, Internat. J. Heat Mass Transfer 15 (1972) 1787–1806.
[19] J.P. Van Doormal, G.D. Raithby, Enhancements of the SIMPLE method for predicting incompressible fluid flows, Numer. Heat Transfer 7 (1984) 147–163.
[20] G.D. Raithby, G.E. Schneider, Numerical solution of problems in incompressible fluid flow: treatment of the velocity-pressure coupling, Numer. Heat Transfer 2 (1979) 417–440.
[21] M.W. Kays, M.E. Crawford, Convective Heat and Mass Transfer, McGraw-Hill Series in Mechanical Engineering, 1993, p. 601.
[22] B. Zeldin, F.W. Schmidt, Developing flow with combined forced-free convection in an isothermal tube, ASME J. Heat Transfer 94 (1972) 211–223.
[23] H. Nesreddine, N. Galanis, C.T. Nguyen, Recirculating flow in aiding/opposing mixed convection in vertical pipes, Numer. Methods Laminar Turbulent Flow 9 (1995) 575–585.